THE JOURNAL OF BIOLOGICAL CHEMISTRY VOL. 287, NO. 17, pp. 13656–13665, April 20, 2012

Crystal Structures of *N*-Acetylmannosamine Kinase Provide Insights into Enzyme Activity and Inhibition*[S]

Received for publication, October 27, 2011, and in revised form, February 14, 2012 Published, JBC Papers in Press, February 16, 2012, DOI 10.1074/jbc.M111.318170

Jacobo Martinez[‡1], Long Duc Nguyen[§1], Stephan Hinderlich[¶2], Reinhold Zimmer[‖], Eva Tauberger[‡], Werner Reutter[§], Wolfram Saenger[‡], Hua Fan[§3], and Sébastien Moniot[‡4]

From the [‡]Institut für Chemie und Biochemie-Kristallographie, Freie Universität Berlin, Takustrasse 6, 14195 Berlin, the [§]Institut für Biochemie und Molekularbiologie, Charité-Universitätsmedizin Berlin, Campus Benjamin Franklin, Arnimallee 22, 14195 Berlin, the [¶]Labor für Biochemie, Fachbereich Life Sciences and Technology, Beuth Hochschule für Technik Berlin, Seestrasse 64, 13347 Berlin, and the [‖]Institut für Chemie und Biochemie-Organische Chemie, Freie Universität Berlin, Takustrasse 3, 14195 Berlin, Germany

Background: UDP-GlcNAc-2 epimerase/ManNAc kinase is the key enzyme for sialic acid biosynthesis.
Results: The crystal structure of ManNAc kinase in complex with its substrate ManNAc has been determined at 1.64 Å resolution.
Conclusion: Insights into the mechanism of ManNAc phosphorylation have been gained from the substrate-bound structure.
Significance: The new structural information presented here offers a basis for designing potential inhibitors of sialic acid biosynthesis.

Sialic acids are essential components of membrane glycoconjugates. They are responsible for the interaction, structure, and functionality of all deuterostome cells and have major functions in cellular processes in health and diseases. The key enzyme of the biosynthesis of sialic acid is the bifunctional UDP-*N*-acetylglucosamine-2-epimerase/*N*-acetylmannosamine kinase that transforms UDP-*N*-acetylglucosamine to *N*-acetylmannosamine (ManNAc) followed by its phosphorylation to ManNAc 6-phosphate and has a direct impact on the sialylation of cell surface components. Here, we present the crystal structures of the human *N*-acetylmannosamine kinase (MNK) domain of UDP-*N*-acetylglucosamine-2-epimerase/*N*-acetylmannosamine kinase in complexes with ManNAc at 1.64 Å resolution, MNK·ManNAc·ADP (1.82 Å) and MNK·ManNAc 6-phosphate·ADP (2.10 Å). Our findings offer detailed insights in the active center of MNK and serve as a structural basis to design inhibitors. We synthesized a novel inhibitor, 6-*O*-acetyl-ManNAc, which is more potent than those previously tested. Specific inhibitors of sialic acid biosynthesis may serve to further study biological functions of sialic acid.

Sialic acids are pyranoses consisting of nine carbon atoms with amino and carboxyl moieties at the C5- and C2-positions, respectively. They are hydrophilic due to their net negative charge conferred by the carboxyl group and are usually present as part of the outermost end of glycan chains of glycoproteins and glycolipids. Because sialic acids are found ubiquitously as terminal components of eukaryotic cell surfaces, they are involved in virtually all interactions of cells with an extracellular matrix or with other cells (1, 2). They serve as recognition sites for various interaction partners or mask antigenic residues from immune surveillance (3, 4).

Sialic acids play a crucial role in human health. In cancer, for example, an altered glycosylation pattern is a universal feature (5, 6), and malignant tumor transformation is associated with increased sialylation levels on tumor cell surfaces, which may serve to protect tumor cells from the recognition by the immune system (7, 8). Overexpression of sialic acid in tumor cells is also associated with a higher metastatic potential (9, 10), which may be a result of stronger interactions between circulating tumor cells with selectins of platelets, leukocytes, and the endothelium (11).

The *de novo* biosynthesis of sialic acid starts with the irreversible transformation of UDP-*N*-acetylglucosamine (UDP-GlcNAc) to *N*-acetylmannosamine (ManNAc) and subsequently to *N*-acetylmannosamine 6-phosphate (ManNAc-6P). These reactions are catalyzed by the bifunctional cytosolic enzyme UDP-GlcNAc 2-epimerase/ManNAc kinase (GNE),[5] which is highly conserved throughout the animal kingdom (12). The activity of GNE is regulated by the downstream product CMP-sialic acid by feedback inhibition (13), which underlines its key role in the sialic acid biosynthetic pathway. Furthermore, GNE overexpression has direct impact on cell surface sialyla-

* This work was supported in part by the Sonnenfeld Stiftung, the Roland and Elfriede Schauer Stiftung, and by DFG-Sonderforschungsbereich 449.
[S] This article contains supplemental Figs. 1–10, Table 1, Data, and an additional reference.
The atomic coordinates and structure factors (codes 2yhw, 2yhy, and 2yi1) have been deposited in the Protein Data Bank, Research Collaboratory for Structural Bioinformatics, Rutgers University, New Brunswick, NJ (http://www.rcsb.org/).
[1] Both authors contributed equally to this work.
[2] Supported by Bundesministerium für Bildung und Forschung and the German-Israeli Foundation for Research and Development.
[3] To whom correspondence may be addressed: Institut für Biochemie und Molekularbiologie, Charité-Universitätsmedizin Berlin, Arnimallee 22, 14195 Berlin-Dahlem, Germany. E-mail: hua.fan@charite.de.
[4] To whom correspondence may be addressed: Dept. of Biochemistry, University of Bayreuth NWI, Universitaetsstrasse 30, 94440 Bayreuth, Germany. Tel.: 92155-2426; Fax: 921552432; E-mail: sebastien.moniot@uni-bayreuth.de.

[5] The abbreviations used are: GNE, UDP-GlcNAc 2-epimerase/ManNAc kinase; h, human; MNK, *N*-acetylmannosamine kinase; AMPPNP, adenosine 5′-(β,γ-imino)triphosphate; ManNAc-6P, ManNAc 6-phosphate; AMPPCP, adenosine 5′-(β,γ-methylenetriphosphate); ITC, isothermal titration calorimetry.

tion (14). In humans, hGNE is related with two genetic diseases, sialuria (15) and hereditary inclusion body myopathy (HIBM). In sialuria, a mutation of either Arg-263 or Arg-266 in the epimerase domain impairs the feedback inhibition of hGNE (16). HIBM is an autosomal recessive neuromuscular disorder caused by more than 60 different point mutations that affect both functional domains of hGNE (17, 18). Given the implication of hGNE in disease and sialic acid biosynthesis, the elucidation of its structure has been a matter of interest. The apostructure of the kinase domain (hMNK) had been already determined by Tong *et al.* (19). We concentrated our efforts in solving the structure of hMNK in its ligand-bound form to characterize the active site and enable the rational design of an inhibitor. Here, we present the crystal structures of the hMNK domain of human GNE in complex with its physiological substrate ManNAc (1.64 Å), in ternary complexes with ManNAc and ADP (1.82 Å) as well as with ManNAc-6P and ADP (2.10 Å). Based on these structures, Asp-517 was presumed to be the catalytic residue. Therefore, the mutants D517N and D517A have been cloned and purified, and their activity was tested. In addition, a set of six HIBM-related mutants were tested in this study. M712T is the main HIBM mutation that occurs compound homozygously in almost all Middle-Eastern patients. N519S, I587T, and A631V were chosen because they also occur compound homozygously in HIBM patients. A631V is also found compound heterozygously in combination with F528C. A631T, a mutation identified in compound heterozygous patients, was chosen due to its similarity to A631V (17, 20, 21).

EXPERIMENTAL PROCEDURES

Cloning and Protein Purification—The DNA fragment coding for hMNK of human GNE1 (amino acids 406–720) was amplified by PCR from plasmid pUMVC3-hGNE1 (12) and cloned into the overexpression vector pET28a (Novagen) with an N-terminal hexahistidine tag cleavable with tobacco etch virus protease or thrombin. Expression in BL21-CodonPlus (DE3)-RIL *Escherichia coli* (Stratagene) was induced at an A_{600} of ~0.5 by the addition of 1 mM isopropyl β-D-thiogalactoside, and the cultures continued to grow for 20 h at 18 °C. The protein was purified at 4 °C by affinity chromatography on a HisTrap 5-ml column (GE Healthcare) using buffer A (20 mM Tris-HCl, pH 8.0, 500 mM NaCl) followed by size-exclusion chromatography using a preparative Superdex S-75 26/60 column (GE Healthcare) and buffer B (10 mM Tris-HCl, pH 8.0, 150 mM NaCl).

HIBM variants of hMNK were prepared similar to wild-type hMNK using pFastBac-hGNE1 constructs (21) with the respective *gne* mutation for variants N519S, F528C, I587T, A631T, and A631V or the pBluescript-hGNE1 construct (22) for variant M712T, as templates for PCR.

Generation of D517A and D517N Mutants—For the production of D517A and D517N point mutations, the "QuikChange™ site-directed mutagenesis kit" of Stratagene was used. pET28a-MNK was applied as template, and the following primers as well as their reverse complement counterpart were chosen: CCCTGTGTGGGTAGACAATGCTGGCAACTGTGCTGCCC for D517A and CCCTGTGTGGGTAGACAATAATGGCAACTGTGCTGCCC for D517N. PCR and cloning were performed following the provider's protocol (Stratagene). The presence of the desired mutation was confirmed by sequencing (Seqlab, Germany).

Activity Assays, hMNK Kinetics, and Inhibition—The kinase activities of recombinant hMNK and all mutants tested in this study were determined spectrophotometrically using an assay containing 60 mM Tris-HCl, pH 8.1, 10 mM $MgCl_2$, 5 mM ManNAc, 10 mM ATP, 0.2 mM NADH, 2 mM phosphoenolpyruvate, 2 units of pyruvate kinase, 2 units of lactate dehydrogenase, and 0.1–1 μg of MNK in a final volume of 200 μl as described previously (23). The reaction was performed for 20 min at 37 °C and stopped by adding 800 μl of 10 mM EDTA. The decrease of NADH was monitored at 340 nm.

The obtained activity was plotted double-reciprocally *versus* substrate concentration, and the K_m value was determined from an average of four independent measurements (supplemental Figs. 1–3).

hMNK kinase activity was measured at 250 μM ManNAc and 5 mM of the indicated inhibitors (*N*-propanoylglucosamine, 3-*O*-Me-GlcNAc, and 6-*O*-Ac-ManNAc). The inhibition was assessed from the reduced activity relative to control without inhibitors. *N*-propanoylglucosamine and 3-*O*-Me-GlcNAc were synthesized and characterized as described earlier (24, 25).

Preparation of 6-O-Acetyl-ManNAc—ManNAc (442 mg, 2 mmol) was dissolved in pyridine (10 ml). *O*-Acetylpropanonoxime (207 mg, 1.8 mmol), 4-Å molecular sieves (100 mg), and lipase AY30 (1.1 g) were added, and the suspension was stirred vigorously at 50 °C. After 5 days, additional lipase AY30 (1.1 g) was added, and the suspension was stirred for an additional 2 days at the same temperature. The lipase was removed by filtration, and the precipitate was washed with MeOH (10 ml). After addition of toluene (15 ml), the solvents were removed by a rotary evaporator; this process was repeated with another 10 ml of toluene, and the resulting crude product was purified by flash chromatography (silica gel, EtOAc/MeOH/H_2O = 25:4:1) to yield 6-*O*-acetyl-ManNAc (18 mg, 4%). The compound was validated by ^1H NMR and high resolution mass spectrometry (ESI-TOF) (supplemental data NMR and ESI-TOF data).

Isothermal Titration Calorimetry—The protein concentration (432 μM for WT-hMNK and 110 μM for D517N MNK) was determined by UV spectroscopy using as absorption coefficient 18450 M^{-1} cm^{-1}. The protein and the ManNAc solution (1 mM) were prepared in ITC buffer (150 mM NaCl, 10 mM Tris, pH 8). The experiments were performed using an ITC 200 (Microcal). 280 μl of protein solution were injected into the calorimeter cell, and the injection syringe was loaded with ManNAc solution. After thermal equilibration at 30 °C and a 1-min initial delay, 20 consecutive injections of 2 μl of ManNAc solution were made into the calorimeter cell under continuous stirring (1000 rpm). The injection spacing was 150 s, which allowed complete re-equilibration. The data were fitted to a one-site model, and the corresponding K_D values were calculated using the software Origin 7 (Microcal) (supplemental Fig. 5).

Crystallization—Crystals of the binary complex hMNK·ManNAc were obtained by co-crystallization using vapor diffusion at 18 °C. The drops were set up by mixing equal volumes

TABLE 1
Data collection and refinement statistics
Values in parentheses refer to the outermost resolution shell.

	MNK/ManNAc	MNK/ManNAc/ADP	MNK/ManNAc-6P/ADP
Data collection			
Beamline	BESSY MX 14.2	BESSY MX 14.2	BESSY MX 14.2
Space group	*P* 41 21 2	*P* 41 21 2	*P* 41 21 2
Unit cell	$a = b = 90.7$; $c = 100.8$ Å	$a = b = 90.4$; $c = 101.2$ Å	$a = b = 90.6$; $c = 101.4$ Å
Nominal resolution	45.3 to 1.64 Å	50.0 to 1.82 Å	41.40 to 2.15 Å
Outermost resolution shell	1.73 to 1.64 Å	1.92 to 1.82 Å	2.27 to 2.10 Å
Unique reflections	52,083% (7584)	38,183 (5567)	23,574 (3484)
Completeness	100% (100%)	100% (100%)	99.7% (100%)
Redundancy	12.9 (12.9)	12.8 (12.9)	11.8 (3.9)
R_{merge}	5.8 (72.5)	5.3 (69.4)	7.9 (64.7)
R_{mrgd}-F	5.9 (39.5)	6.0 (40.9)	9.3 (44.6)
Mean $I/\sigma(I)$	30.66 (4.37)	34.07 (4.40)	24.52 (4.0)
Refinement			
R_{work}/R_{free}	14.8/17.0%	15.2/18.2%	17.2/20.0%
Root mean square from ideal geometry			
Bond lengths	0.026 Å	0.025 Å	0.022 Å
Bond angles	2.068°	2.097°	1.788°
Dihedral angles	6.637°	6.180°	6.465°
Chiral center restraints	0.157	0.128	0.108
Mean B factor (Å^2)			
Overall model	25.7	31.6	37.1
Protein atoms	25.2	30.8	37.0
Sugar	12.5	16.2	18.7 (ManNAc) 23.4 (ManNAc-6P)
ADP		58.0	66.3
PDB ID	2YHW	2YHY	2YI1

(2 μl) of 15 mg/ml protein and 2 mM ManNAc in buffer B and screen reservoir solution (0.2 M calcium acetate, 0.1 M sodium cacodylate, pH 6.5, and 40% PEG 300). Diamond-shaped crystals reached their maximal size within 5 days and were directly flash-frozen in liquid nitrogen prior to data collection. No crystals could be obtained by co-crystallization of hMNK with ManNAc and ADP, ATP, AMPPCP, or AMPPNP, but ternary complexes were obtained by soaking crystals of the binary hMNK·ManNAc complex replacing stepwise their mother liquor with solutions containing 0.1 M sodium cacodylate, pH 6.5, 50% PEG 300, and 20 mM ADP or ATP or nonhydrolyzable ATP derivatives.

X-ray Diffraction Data Collection and Structure Refinement—X-ray diffraction data were collected at 100 K on beamline BL 14.2 (BESSY, Berlin). The data were integrated, reduced, and scaled using XDS/XSCALE (26). Statistics of the crystallographic data are summarized in Table 1. The structure of the hMNK·ManNAc complex was solved by molecular replacement using MOLREP (27) of the CCP4 program suite (28) and a monomer from the apo-form structure of hMNK as search model (19) (PDB code 3EO3). The ternary complex structures were solved by molecular replacement using the hMNK·ManNAc structure as search model.

The asymmetric unit contains one hMNK monomer that was subjected to rigid-body refinement, followed by iterative cycles of TLS and restrained-maximum likelihood refinement, including isotropic temperature factor adjustment with REFMAC (29) and manual rebuilding using COOT (30). During this process, 5% randomly selected reflections were used to calculate R_{free}. Water molecules were added using COOT, and the models were validated using MOLPROBITY (31). Statistics concerning the refinement and geometry of the structures are summarized in Table 1. Atomic coordinates and structure factors have been deposited in the Protein Data Bank under codes 2yhw, 2yhy, and 2yi1.

RESULTS

Enzymatic Properties of hMNK—The specific activity of recombinant hMNK for ManNAc was found to be 2.6 units/mg protein, which is comparable with the corresponding kinase activity of full-length hGNE (2.4 units/mg) (21). Kinetic experiments revealed the K_m values for ManNAc to be 95 μM and for ATP to be 4.4 mM (supplemental Figs. 1 and 2).

Overall Structure of the hMNK Monomer—The high quality of the electron density maps at 1.64 Å resolution allowed the building of the model for ManNAc and hMNK. No electron density could be attributed to residues 617–620, which are consequently missing in the final model. The overall fold of hMNK is composed of two lobes arranged like a "V," with each leg of the V representing one of the lobes (Fig. 1, *a* and *b*). Both lobes are connected by a hinge composed of two flexible loops (amino acids 529–535 and 700–702) allowing hMNK to change from an open conformation to a closed one upon substrate binding (see below). The interface between the two lobes (at the inner bottom side of the V) defines a large cavity containing the active site, where ManNAc and ATP bind (Fig. 1, *a* and *b*).

Dynamics of Substrate Binding and Multimeric State of hMNK—A comparison of the apo-hMNK structure (19) with the structure of the hMNK·ManNAc complex using DYNDOM (32) showed a clear conformational change of the V-shaped protein (Fig. 1*e*). Upon substrate binding, the N-terminal lobe rotates 12° toward the C-terminal lobe. This closure allows hMNK to embrace and tightly coordinate ManNAc. Both lobes behave as rigid bodies, and the flexibility is conferred by the hinge. The protein fold of the hMNK·ManNAc complex is, however, not significantly modified by ADP or ATP binding.

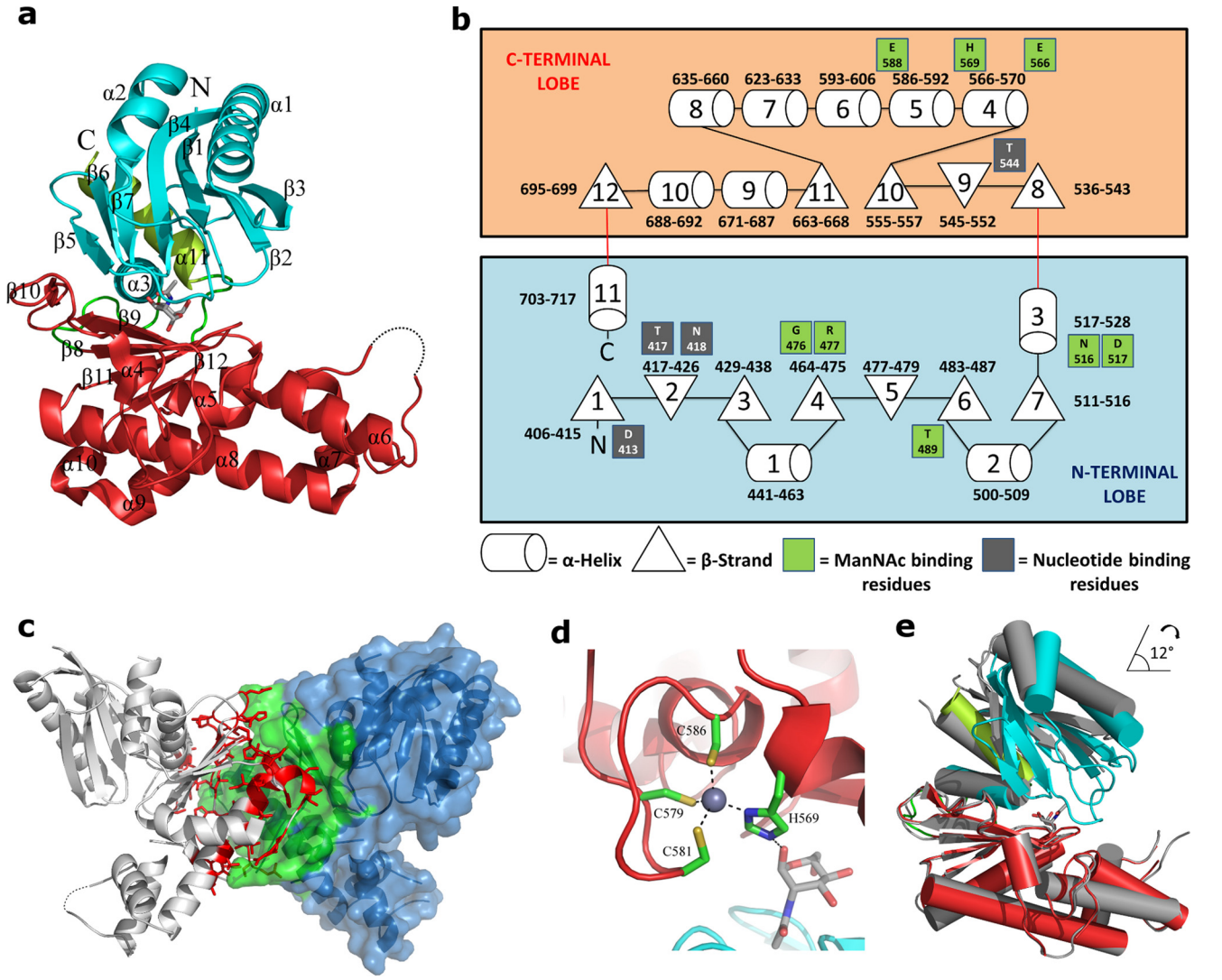

FIGURE 1. *a,* ribbon representation of the human ManNAc kinase domain monomer in complex with its natural substrate. The N-terminal lobe is shown in *blue*, and the C-terminal lobe is in *red*. ManNAc is depicted as *gray sticks*. The secondary structure elements are labeled as α (helices) or β (strands) followed by a number indicating their occurrence in the primary structure. The C-terminal α-helix (α11) protrudes out of the C-terminal lobe into the N-terminal lobe and is in *green* for clear orientation. The *dashed line* in the loop connecting α6 with α7 indicates a flexible unmodeled region. *b,* schematic representation of the hMNK topography. The two lobes are *boxed* and *colored* according to *a* and connected by *two red lines* indicating the hinge regions. The *numbers* close to each secondary structure elements indicate the N- and C-terminal amino acids. The residues forming the ManNAc and the ADP-binding sites are shown in *green* and *gray rectangles*, respectively. *c,* presentation of the hMNK homodimer. The physiological dimer of hMNK was reconstituted from monomer A using the relevant crystallographic 2-fold axis. Monomers A and A′ are displayed in *white* (ribbon) and *blue* (ribbon and surface) with their interfacing residues (1760 Å^2) in *red* and *green*, respectively. *d,* zinc-binding site. The tetrahedral coordination of Zn^{2+} (*gray sphere*) concerns three cysteine residues (sulfur atoms in *yellow*) and a histidine (nitrogen in *blue*). Upon metal binding, His-569 adopts the correct orientation for the coordination of the ManNAc-O^1 atom. *e,* superimposition of the C-terminal lobes from hMNK/ManNAc and the apo-hMNK structures (the apo-hMNK in *gray*, PDB code 3EO3). The helices are displayed as *cylinders* for clarity. Upon ManNAc binding, the N-lobe (*blue*) pivots 12° toward the C-lobe (*red*) about the hinge region (*green loops*). This clearly differentiates the open apo-hMNK (*gray*) from the closed ligand-bound conformation (*blue* and *red*).

The crystal asymmetric unit harbors one hMNK/ManNAc, and examination of the crystal structure using PISA (33) revealed a biologically relevant homodimer formed by two symmetry-related molecules sharing a contact interface of 1760 Å^2 (Fig. 1*c*). All amino acids implied in dimerization belong to the C-terminal lobe of hMNK and create an intricate network of 30 hydrogen bonds stabilizing the quaternary structure of the hMNK dimer. The N-terminal lobe is not implicated in dimerization and possesses more freedom, which allows it to undergo the necessary conformational changes to bind ManNAc. A similar analysis of the dimer in apo-hMNK (19) shows a monomer-monomer interface of only 1587 Å^2 that is stabilized by 22 hydrogen bonds, indicating that substrate binding to hMNK contributes significantly to the stabilization of the quaternary structure. The dimeric character of hMNK observed in the crystal structures correlates with the retention times obtained by size-exclusion chromatography (supplemental Fig. 6).

Zn^{2+}-binding Site—A Zn^{2+} is located between α4 and α5 and tetrahedrically coordinated by Cys-579, Cys-581, and Cys-586 with Zn^{2+}-Sγ distances of 2.35, 2.33, and 2.26 Å, respectively, and His-569 arising from the loop between these two α-helices with distance Zn^{2+}-$N^{\delta1}$(His-569) of 2.11 Å (Fig. 1*d*). The four residues implied in Zn^{2+} binding are part of the specific ROK family motif signature (34). The B factor for Zn^{2+} (14.5 Å^2) correlates with the B factor of the atoms in its direct

environment (15.0 $Å^2$ on average) and suggests full occupancy, although no Zn^{2+} was added during purification. This indicates an endogenous strong binding of Zn^{2+} whose structural role is critical in defining the topography of the active center.

ManNAc-binding Site—The Fourier difference maps of the hMNK·ManNAc complex clearly show the presence of the α-anomeric form of ManNAc in $^4C_1$ chair conformation in the active site of hMNK. The average B factor for ManNAc is 12.2 $Å^2$, even lower than the average B factor for the main chain of MNK (14.3 $Å^2$), and indicates that the sugar-binding site is fully occupied.

All the polar atoms of ManNAc are hydrogen-bonded by eight surrounding amino acids of hMNK and three water molecules that form a network of 17 hydrogen bonds. The N-terminal lobe is the major contributor to this network with five amino acids (Gly-476, Arg-477, Thr-489, Asn-516, and Asp-517), and the other three residues belong to the C-terminal lobe of hMNK (Glu-566, His-569, and Glu-588).

The hydrogen bonding network binding ManNAc is displayed in Fig. 2*a*, and the interactions are summarized in Table 2. Gly-476 and Arg-477 are situated in the loop connecting β4 with the hairpin β-sheet formed by β5 and β6, and Thr-489 belongs to the loop following β6. The short loop connecting β7 and helix α3 bears the other two residues, Asn-516 and the presumed catalytic residue Asp-517, that are located in the N-terminal lobe.

The active center residues of the C-terminal lobe seem to be orientated by the Zn^{2+}-binding motif. This is especially evident for His-569, whose $N^{\delta1}$ and $N^{\epsilon2}$ atoms directly coordinate both Zn^{2+} and the ManNAc-O^1 atom, respectively. Glu-566 and Glu-588, which are two of the ManNAc-binding residues, are close to His-569 and Cys-586, respectively, and underline the central role of the Zn^{2+}-binding motif for the active center of MNK.

Nucleotide-binding Site—Because attempts to co-crystallize hMNK with ManNAc and ADP, ATP, or AMPPCP were unsuccessful, crystals of the binary complex hMNK·ManNAc were soaked either with ATP or ADP. The structure of the ternary complex between MNK, ManNAc, and ADP could be determined at 1.82 Å resolution (Table 1 and Fig. 2*b*). The electron density difference maps clearly showed the presence and position of the α- and β-phosphate groups of ADP as well as of the Mg^{2+} necessary for catalysis. The ribose moiety was partially defined, but no electron density was found for the adenine moiety, which is probably due to weak coordination and high flexibility of the nucleotide-binding site, as also indicated by the K_m of 4.4 mM for ATP.

Prolonged soaking of hMNK/ManNAc crystals with ATP afforded the structure of the ternary complex hMNK·ManNAc-6P·ADP that was determined at 2.10 Å resolution (Fig. 2*c*). In this case also, no electron density could be found for the adenine moiety of ADP; however, additional electron density extending from the ManNAc-O^6 atom was attributed to the partial presence of the phosphorylated product of the reaction, ManNAc-6P (0.4 occupancy) in coexistence with the substrate ManNAc (0.6). This indicates that the kinase reaction has taken place in the crystal and that the γ-phosphate of ATP has been transferred to ManNAc.

The β-phosphate of ADP is stabilized by a total of eight interactions (Fig. 2*b*). On one side, the β-phosphate interacts with the backbone NH of Thr-417, Asn-418, and Thr-544, as well as with Thr-544-$O^{\gamma1}$. On the other side, the β-phosphate is stabilized by hydrogen bonds to three water molecules that are further hydrogen-bonded to ManNAc-O^6H and the NH group of Gly-545 (water molecule number **1** in Fig. 2*b*), Asp-413-$O^{\delta1}$, and Asp-517-$O^{\delta1}$ (water molecule number **2**), and to Arg-420-$N^{\eta2}$ (water molecule number **3**).

Mg^{2+} is octahedrically coordinated with the β-phosphate-O^3 atom and Asp-413-$O^{\delta2}$ in the axial positions, whereas four water molecules occupy the equatorial sites. The side chain of Asp-413 does not directly bind one of the oxygens of the β-phosphate but is necessary for Mg^{2+} coordination and consequently crucial for ATP binding.

The α-phosphate of ADP is mainly coordinated by the side chains of Arg-420-$N^{\eta1}$ and Asn-418-$N^{\delta2}$ and is further stabilized by two water-mediated hydrogen bonds (water molecules **3** and **4**). All the amino acids involved in pyrophosphate coordination are located within strand β2 of the N-terminal lobe (Thr-417, Asn-418, and Arg-420) and in the loop connecting β8 and β9 of the C-terminal lobe (Thr-544).

In the hMNK·ManNAc·ADP complex, the $O^{3'}$H group of ADP is only stabilized by a hydrogen bond to Gln-597-$O^{\epsilon1}$ that is mediated by water molecule number **5** (Fig. 2*b*). In the ternary complex hMNK·ManNAc-6P·ADP, however, $O^{3'}$H of ADP engages in two direct hydrogen bonds with Thr-417-$O^{\gamma1}$ and Thr-544-$O^{\gamma1}$, and $O^{2'}$H is stabilized by a water-mediated hydrogen bond to the side chain of Gln-597 (Fig. 2*c*).

Catalytic Role of Asp-517—Based on the hMNK/ManNAc structure Asp-517 was presumed to exert a catalytic role, due to its proximity to the ManNAc-6OH and to its high conservation among homologous sugar kinases (Fig. 2*a* and supplemental Table 1). To validate this hypothesis, the variants D517A and D517N were prepared, and their enzymatic activity was tested. In both cases, no activity could be detected (Table 3). Furthermore, to elucidate whether the MNK inactivation was due to a missense folding induced by the mutation of Asp-517, the secondary structure content of WT-hMNK, D517A, D517N, and a set of six HIBM-related mutants was analyzed by CD spectra (Table 3). No major differences were found for the variant D517N, whereas D517A showed a small yet insignificant increase for the random coil content with respect to the wild type (38% *versus* 40%). A closer observation of Table 3 reveals that among all variants, D517A and D517N show the smallest secondary structure content variation with respect to the wild type. These data suggest that the loss of activity for the Asp-517 variants (Table 3) is rather related to the specific catalytic role of this amino acid than to the effect of this single point mutation on the overall fold of the enzyme. Because Asp-517 is also involved in ManNAc coordination, it was important to find out whether the mutations impaired sugar binding. The dissociation constants (K_D) for wild type (WT)-hMNK/ManNAc (2.5 μM) and D517N/ManNAc (259 μM) were determined by ITC. D517N shows 100-fold lower affinity compared with WT-MNK, but this binding affinity would still be sufficient for normal enzyme activity. All other variants tested in this study showed a weaker binding, and no K_D value could be evaluated

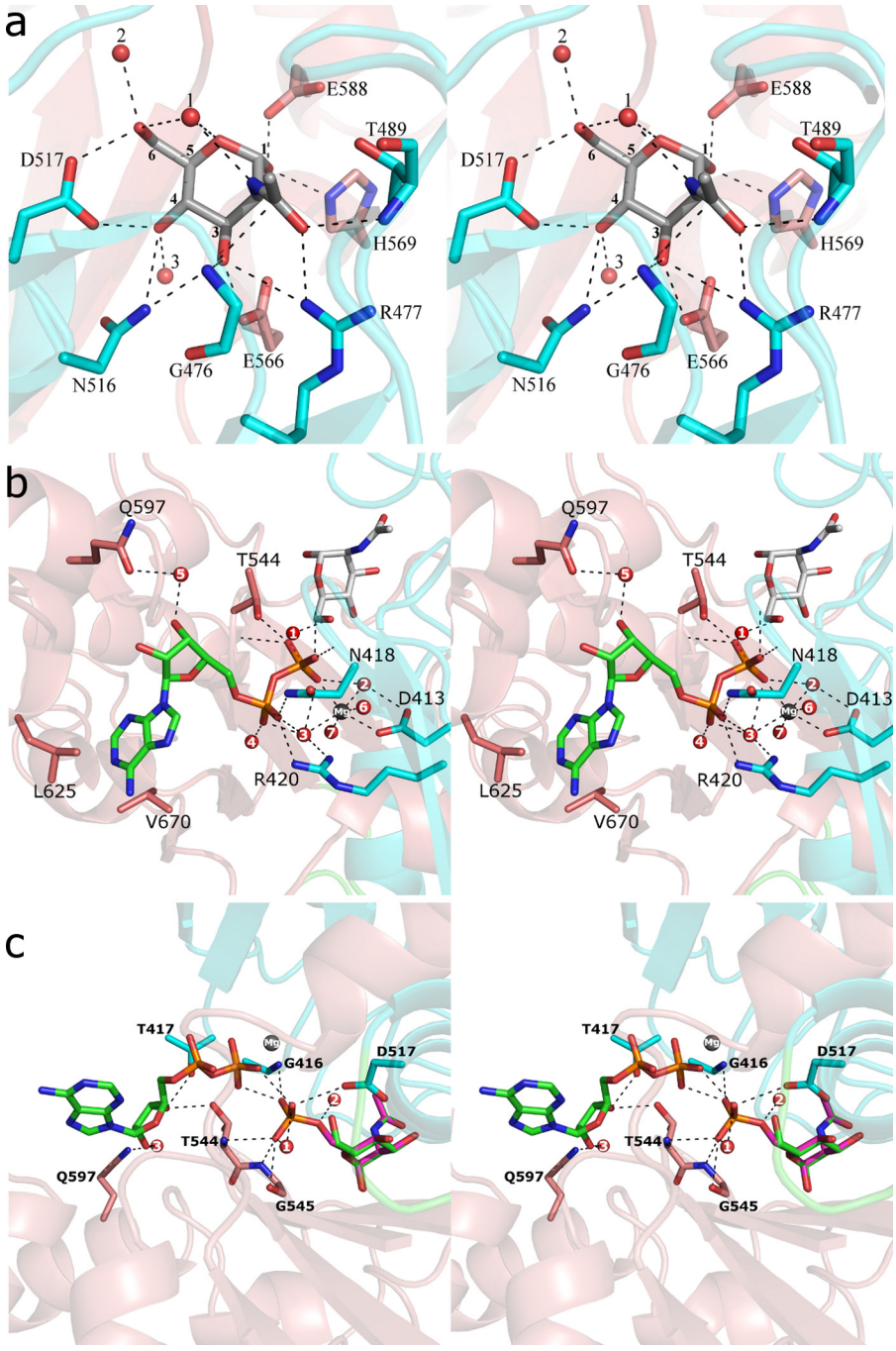

FIGURE 2. *a,* stereo view of the ManNAc-binding site. The colors of the secondary structures are consistent with Fig. 1*a* indicating whether the residues arise from the N-terminal lobe (*blue*) or from the C-terminal one (*red*). The residues involved in ManNAc binding are represented as *sticks*, ManNAc atoms are *numbered*. Oxygen and nitrogen atoms are displayed in *red* and *blue*, respectively. The three water molecules are shown as *red spheres* and *numbered*. *Broken lines* show the extensive hydrogen bond network between hMNK and ManNAc. *b,* stereo view of the ADP-binding site. The colors of the secondary structures are consistent with Fig. 1, *a* and *b*. Oxygen and nitrogen atoms are displayed in *red* and *blue*, respectively. The seven water molecules involved in ADP binding are displayed as *red spheres* and numbered in *white*. *Broken lines* show hydrogen bonds. ADP is shown in *green* (adenine moiety and ribose) and *orange* (phosphates). Mg^{2+} (*gray sphere*) is octahedrally coordinated, axially between Asp-413 and the β-phosphate O^3 and equatorially by four water molecules (2, 3, 6, and 7). The ManNAc molecule is also shown (C atoms *white*, in the back of the picture), hydrogen-bonded with O^6H to water molecule 1. This gives a first impression of the distance separating the β-phosphate and the sugar phosphorylation site, hydroxyl O^6H. *c,* stereo view of the ManNAc-6P phosphate coordination. The color coding of the secondary structure elements is consistent with Fig. 1, *a* and *b*. Oxygen and nitrogen atoms are displayed in *red* and *blue*, respectively. Water molecules involved are displayed as *red spheres* and numbered in *white*. *Broken lines* show the hydrogen bond network surrounding the phosphate (*orange*) at the O-6 position. The ManNAc-6P molecule (0.4 occupancy) is displayed with lilac backbone, and the unphosphorylated ManNAc molecule (0.6 occupancy) is shown in *green*. *b* and *c,* adenine moiety has been modeled in a plausible conformation becauseit was not defined in the electron density maps (see supplemental Fig. 10). *O6H*, the hydroxyl function located on the 6th position of the ribose ring.

by ITC. Interestingly, all other variants except D517N and D517A have partial enzymatic activity, confirming the catalytic role of Asp-517 in hMNK.

HIBM Mutation Analysis—The only genetic determinants of HIBM pathology are defined mutations of hGNE (17). Mutations on one functional domain can also affect the enzymatic

TABLE 2
Hydrogen bond contacts for ManNAc

Sugar atom	Protein atom	Distance
		Å
ManNAc O1	His-569-$N^{\epsilon 2}$	2.7
	Glu-588-$O^{\epsilon 1}$	2.55
ManNAc N2	Water-1	3.0
ManNAc O3	Gly-476-N	2.9
	Arg-477-$N^{\eta 2}$	3.2
	Glu-566-$O^{\epsilon 2}$	2.6
	Asn-516-$N^{\delta 2}$	3.1
ManNAc O4	Asn-516-$N^{\delta 2}$	3.2
	Water-3	2.8
	Asp-517-$O^{\delta 2}$	2.6
ManNAc O6	Asp-517-$O^{\delta 1}$	2.6
	Water-2	2.7
	Water-1	2.9
ManNAc O5	Water-1	3.2
ManNAc carbonyl	Thr-489-N	2.9
	Arg-477-$N^{\eta 2}$	2.9

TABLE 3
Secondary structure content for HIBM-related mutants determined by CD spectroscopy and their relative specific activity

	α-Helix	β-Sheet	β-Turn	Random coil	Relative specific activity
MNK	20	24	18	38	100
D517A	16	26	18	40	0
D517N	23	22	18	37	0
N519S	15	27	18	40	25
F528C	10	31	18	41	78
I587T	11	30	18	41	24
A631T	10	31	17	42	4
A631V	12	29	17	42	26
M712T	11	30	17	42	40

activity of the other domain (21). The cellular mechanism linking these mutations to muscle degeneration is still unknown. To understand the structural implications of mutations that are associated with HIBM, the hMNK domains of six HIBM-related hGNE variants were cloned, purified, characterized, and compared with WT-hMNK (Table 3). An extensive structural mapping of these disease-associated mutations has been previously performed by Tong *et al.* (19) based on the apo-hMNK structure. Here, we focus on the six point mutations that had been biochemically characterized in this work (Table 3) and use the newly gained structural information (residues involved in ManNAc and ATP binding) to discuss the structural implication of these mutations in hMNK activity.

Given the highly compact fold of hMNK, it is understandable that many single point mutations are prone to disrupt hMNK architecture. Asn-519 is located on helix α3, and Asn-519-$N^{\delta 2}$ is hydrogen-bonded to Asp-515-$O^{\delta 1}$, thereby orientating Asn-516 and Asp-517, two of the sugar-binding residues. A mutation to serine (N519S) alters this interaction and consequently the binding affinity of the sugar. Phe-528 is located at the very C terminus of helix α3 in a hydrophobic contact interface with strand β11. The exchange of phenylalanine with a smaller polar residue like cysteine (F528C) might disrupt this interaction and affect the orientation of the sugar-binding residues at the C-terminal part of α3. Ile-587 is buried and inaccessible to solvent. Its location between Cys-586 (Zn^{2+}-binding) and Glu-588 (sugar-binding) suggests that a change of Ile-587 to a polar residue like threonine will disturb the binding of both Zn^{2+} and ManNAc. Ala-631 is located at the C terminus of helix α7 in an area of poorly defined electron density, making the orientation of alanine unreliable. Because Ala-631 is far away from the sugar-binding site, a mutation of this residue would rather impair ATP binding, which fits with the low enzymatic activity observed for the two variants A631T and A631V (Table 3) and the conservation of the high specificity for ManNAc. Met-712 on helix α11 forms hydrophobic contacts with β4 and β7 that bear four of the sugar-binding residues in two loops at their respective C termini (Gly-476 and Arg-477 for β4 and Asn-516 and Asp-517 for β7). In the variant M712T, because threonine is shorter than methionine, these interactions are disturbed, which would explain the implications of this mutation, *i.e.* reduced α-helix content to 11%, increased β-strand content to 30%, and enzymatic activity reduced to 40%, compared with WT-hMNK (Table 3).

MNK Inhibition—With the known crystal structures, it is now possible to design hMNK inhibitors using molecular modeling techniques. Based on the geometry of the active center of hMNK, we postulated that modifications at the C6-position of ManNAc could yield potential inhibitors. *N*-Propanoylglucosamine and 3-*O*-Me-GlcNAc were described in previous studies to inhibit MNK activity in cell lysates (24, 25). The inhibition effect of these substances was tested in this study with purified recombinant hMNK. At 5 mM inhibitor concentration, the activity of hMNK was only decreased by 17 and 26%, respectively, for these two compounds (supplemental Fig. 4). We synthesized 6-*O*-Ac-ManNAc that has a significantly stronger inhibitory effect of 60% at 5 mM inhibitor concentration with a measured K_i of 1.4 mM (supplemental Fig. 4).

DISCUSSION

The elucidation of the crystal structure of hMNK in complex with ManNAc revealed that upon substrate binding, hMNK undergoes structural changes from an open substrate-free conformation (19) to a closed sugar-bound one. This "induced fit" is a common feature of sugar kinases like human *N*-acetylglucosamine kinase (35) or hexokinase from *Sulfolobus tokodaii* (36). Only for YdhR, a closely related fructokinase from *Bacillus subtilis,* also belonging to the ROK family, no major structural changes upon fructose binding have been described (37). However, this is likely to be a crystallographic artifact, where the crystal packing induces the close conformation. Indeed, time-resolved fluorescence studies on adenylate kinase suggested that there is not only an open and a close conformation but that substrate binding contributes to trap the protein in a so-called "closed" conformation, which otherwise exists also in solution (38). The loop containing Thr-417, an amino acid involved in nucleotide binding, differs by 5 Å within apo- and ligand-bound structures (supplemental Fig. 7), clearly indicating that the conformational change induced by the binding of ManNAc is a prerequisite for ATP binding. This is meaningful in a biological context because it prevents hMNK from unnecessary wasting ATP in absence of substrate.

The high affinity (K_m of 95 μM) of hMNK for ManNAc correlates with the dense hydrogen bond network that hMNK uses to bind ManNAc (Fig. 2*a* and Table 2). Also, the relatively low affinity (K_m of 4.4 mM) of hMNK for ADP correlates with the

less well defined hydrogen bond network found for this interaction (Fig. 2*b*).

hMNK is the first human member of the ROK family (39) to be structurally characterized in complex with its specific substrate. We found that the Zn^{2+}-binding motif (40) (common signature to all ROK family members) is necessary to properly orientate several residues of the active center, thus playing a structural key role for the enzymatic activity of hMNK, which is particularly evident for His-569, which coordinates both, Zn^{2+} and the C1 hydroxyl group of ManNAc. This phenomenon had been already observed for other members of the ROK family. In the fructokinase YdhR, His-153 interacts with the C1 hydroxyl group from D-fructose and complexes Zn^{2+} simultaneously (37). Furthermore, mutations of the cysteine residues of the motif have been shown to inactivate the *B. subtilis* glucokinase activity (41) and reduction of the function of the Mlc repressor (34) underlying the importance of the motif for protein activity.

The apo-hMNK crystal structure featured a crystallographic hexamer formed by interaction between the N-terminal lobes of symmetry-related mates, which was discussed by the authors to be biologically relevant (19). However, our findings suggest that this is a crystallographic artifact rather than a naturally occurring multimer, because this arrangement would reduce the flexibility of the N-terminal lobe that appears to be required for substrate binding. Our crystal structures clearly display hMNK in a dimeric form (Fig. 1*c*), which is in concordance with the retention time obtained by size-exclusion chromatography (supplemental Fig. 6). Ghaderi *et al.* (42) previously demonstrated that FL-GNE can exist as a fully active tetramer or as a dimer possessing only kinase activity. Taken together, these data suggest that the kinase domain of hGNE is responsible for dimerization, and the epimerase domain assemble two dimers to form the fully active GNE tetramer.

In the hMNK·ManNAc·ADP complex, the adenine moiety has been modeled in a hydrophobic pocket where it is stacked between the side chains of Leu-625 and Val-670 (Fig. 2*b*). The conformation of both the ribose and the adenine moieties observed here is consistent with the one observed for AMPPNP in the crystal structure of human glucokinase (43) and ADP in the crystal structure of fructokinase YdhR from *B. subtilis* (37). The conformation of adenine is different in the complex with ManNAc-6P, its plane being rotated by ~100°, and it stacks on top of Leu-625 and Val-670. In both complexes, the adenine moiety is poorly defined in electron density maps that, as well as its conformational variability, reflect flexibility of this moiety. One possible explanation could be the relatively low binding affinity of hMNK for ATP (K_m of 4.4 mM); however, it cannot be excluded that further spatial rearrangements could occur in solution to properly accommodate the nucleotide and especially the adenine base.

The catalytic role of Asp-517 for hMNK could be confirmed by point mutations and enzymatic tests (see "Results" and Table 3). Analogous to other kinases (44–46), the expected chemical mechanism implies a nucleophilic attack of the O^6 atom of the substrate ManNAc on the γ-phosphorus atom of the ATP molecule. The nucleophilicity of the O^6 atom from the alcohol group at the C6 atom is increased by deprotonation. For this purpose, the catalytic residue Asp-517 acts as a general base. Asp-517-$O^{\delta 1}$ and ManNAc-O^6 are in hydrogen bond distance (2.6 Å) and well oriented with respect to each other (supplemental Fig. 8).

Given the known alterations in the sialylation pattern of tumor cell surfaces (5–8), the search for an inhibitor of sialic acid biosynthesis is a matter of great biochemical interest. An inhibitor would provide a valuable tool for research on hitherto unknown functions of sialic acid in membrane glycoconjugates or in serum constituents. Furthermore, inhibition of sialic acid biosynthesis could render metastatic cells more susceptible to the immune system, because most metastatic cells are protected by a sialic acid shield from immune recognition (47). Because hGNE is the key enzyme in sialic acid biosynthesis and its impairment diminishes the level of sialic acid expression on cell surfaces (14), many UDP-GlcNAc and transition state analogs were synthesized as inhibitors for the epimerase activity of hGNE and tested to date (48, 49). However, because of their hydrophilic nature, these inhibitors cannot penetrate the cell plasma membrane and are ineffective in cellular systems. hMNK could be another target for the inhibition of the pathway. Even if some alternative pathways for ManNAc phosphorylation are known (50) and the direct conversion of ManNAc into Neu5Ac has been reported (51, 52), the inhibition of the kinase could at least diminish the yield of sialic acid production.

Because ManNAc is closely engulfed into the substrate binding pocket of hMNK and only the hydroxyl moiety at the C6 position is sterically accessible (supplemental Fig. 9), we hypothesized that a modification of the C6-position of ManNAc with a relatively small polar group could yield a potential hMNK inhibitor. As a proof of principle, 6-*O*-Ac-ManNAc was synthesized and found to competitively inhibit hMNK stronger than all other previously published inhibitors of hMNK (24, 25). The crystal structures presented here provide the basis for the rational design of new inhibitors of hMNK.

Acknowledgments—We acknowledge access to beamline BL14.2 of the BESSY II storage ring (Berlin, Germany) via the Joint Berlin MX-Laboratory sponsored by the Helmholtz Zentrum Berlin für Materialien and Energie, Freie Universität Berlin, Humboldt-Universität zu Berlin, Max-Delbrück Centrum, and Leibniz-Institut für Molekulare Pharmakologie. We thank Johannes Schwan and Prof. H.-U. Reissig for help in 6-O-Ac-ManNAc synthesis.

REFERENCES

1. Schauer, R. (2004) Sialic acids. Fascinating sugars in higher animals and man. *Zoology* **107,** 49–64
2. Varki, A. (2007) Glycan-based interactions involving vertebrate sialic acid-recognizing proteins. *Nature* **446,** 1023–1029
3. Kelm, S., and Schauer, R. (1997) Sialic acids in molecular and cellular interactions. *Int. Rev. Cytol.* **175,** 137–240
4. Varki, A. (1997) Sialic acids as ligands in recognition phenomena. *FASEB J.* **11,** 248–255
5. Kim, Y. J., and Varki, A. (1997) Perspectives on the significance of altered glycosylation of glycoproteins in cancer. *Glycoconj. J.* **14,** 569–576
6. Chen, S., and Fukuda, M. (2006) Cell type-specific roles of carbohydrates in tumor metastasis. *Methods Enzymol.* **416,** 371–380
7. Bhavanandan, V. P. (1991) Cancer-associated mucins and mucin-type glycoproteins. *Glycobiology* **1,** 493–503
8. Raval, G. N., Patel, D. D., Parekh, L. J., Patel, J. B., Shah, M. H., and Patel, P. S. (2003) Evaluation of serum sialic acid, sialyltransferase, and sialopro-

teins in oral cavity cancer. *Oral Dis.* **9,** 119–128
9. Bresalier, R. S., Rockwell, R. W., Dahiya, R., Duh, Q. Y., and Kim, Y. S. (1990) Cell surface sialoprotein alterations in metastatic murine colon cancer cell lines selected in an animal model for colon cancer metastasis. *Cancer Res.* **50,** 1299–1307
10. Sawada, R., Tsuboi, S., and Fukuda, M. (1994) Differential E-selectin-dependent adhesion efficiency in sublines of a human colon cancer exhibiting distinct metastatic potentials. *J. Biol. Chem.* **269,** 1425–1431
11. Varki, N. M., and Varki, A. (2002) Heparin inhibition of selectin-mediated interactions during the hematogenous phase of carcinoma metastasis. Rationale for clinical studies in humans. *Semin. Thromb. Hemost.* **28,** 53–66
12. Reinke, S. O., Lehmer, G., Hinderlich, S., and Reutter, W. (2009) Regulation and pathophysiological implications of UDP-GlcNAc 2-epimerase/ManNAc kinase (GNE) as the key enzyme of sialic acid biosynthesis. *Biol. Chem.* **390,** 591–599
13. Kornfeld, S., Kornfeld, R., Neufeld, E. F., and O'Brien, P. J. (1964) The feedback control of sugar nucleotide biosynthesis in liver. *Proc. Natl. Acad. Sci. U.S.A.* **52,** 371–379
14. Keppler, O. T., Hinderlich, S., Langner, J., Schwartz-Albiez, R., Reutter, W., and Pawlita, M. (1999) UDP-GlcNAc 2-epimerase. A regulator of cell surface sialylation. *Science* **284,** 1372–1376
15. Weiss, P., Tietze, F., Gahl, W. A., Seppala, R., and Ashwell, G. (1989) Identification of the metabolic defect in sialuria. *J. Biol. Chem.* **264,** 17635–17636
16. Eisenberg, I., Avidan, N., Potikha, T., Hochner, H., Chen, M., Olender, T., Barash, M., Shemesh, M., Sadeh, M., Grabov-Nardini, G., Shmilevich, I., Friedmann, A., Karpati, G., Bradley, W. G., Baumbach, L., Lancet, D., Asher, E. B., Beckmann, J. S., Argov, Z., and Mitrani-Rosenbaum, S. (2001) The UDP-*N*-acetylglucosamine 2-epimerase/*N*-acetylmannosamine kinase gene is mutated in recessive hereditary inclusion body myopathy. *Nat. Genet.* **29,** 83–87
17. Huizing, M., and Krasnewich, D. M. (2009) Hereditary inclusion body myopathy. A decade of progress. *Biochim. Biophys. Acta* **1792,** 881–887
18. Argov, Z., and Mitrani-Rosenbaum, S. (2008) The hereditary inclusion body myopathy enigma and its future therapy. *Neurotherapeutics* **5,** 633–637
19. Tong, Y., Tempel, W., Nedyalkova, L., Mackenzie, F., and Park, H. W. (2009) Crystal structure of the *N*-acetylmannosamine kinase domain of GNE. *PLoS One* **4,** e7165
20. DeLano, W. L. (2010) *The PyMOL Molecular Graphics System,* Version 1.3rl, Schrödinger, LLC, New York
21. Penner, J., Mantey, L. R., Elgavish, S., Ghaderi, D., Cirak, S., Berger, M., Krause, S., Lucka, L., Voit, T., Mitrani-Rosenbaum, S., and Hinderlich, S. (2006) Influence of UDP-GlcNAc 2-epimerase/ManNAc kinase mutant proteins on hereditary inclusion body myopathy. *Biochemistry* **45,** 2968–2977
22. Hinderlich, S., Salama, I., Eisenberg, I., Potikha, T., Mantey, L. R., Yarema, K. J., Horstkorte, R., Argov, Z., Sadeh, M., Reutter, W., and Mitrani-Rosenbaum, S. (2004) The homozygous M712T mutation of UDP-*N*-acetylglucosamine 2-epimerase/*N*-acetylmannosamine kinase results in reduced enzyme activities but not in altered overall cellular sialylation in hereditary inclusion body myopathy. *FEBS Lett.* **566,** 105–109
23. Hinderlich, S., Stäsche, R., Zeitler, R., and Reutter, W. (1997) A bifunctional enzyme catalyzes the first two steps in *N*-acetylneuraminic acid biosynthesis of rat liver. Purification and characterization of UDP-*N*-acetylglucosamine 2-epimerase/*N*-acetylmannosamine kinase. *J. Biol. Chem.* **272,** 24313–24318
24. Grünholz, H. J., Harms, E., Opetz, M., Reutter, W., and Cerný, M. (1981) Inhibition of *in vitro* biosynthesis of *N*-acetylneuraminic acid by *N*-acyl- and *N*-alkyl-2-amino-2-deoxyhexoses. *Carbohydr. Res.* **96,** 259–270
25. Zeitler, R., Giannis, A., Danneschewski, S., Henk, E., Henk, T., Bauer, C., Reutter, W., and Sandhoff, K. (1992) Inhibition of *N*-acetylglucosamine kinase and *N*-acetylmannosamine kinase by 3-*O*-methyl-*N*-acetyl-D-glucosamine *in vitro*. *Eur. J. Biochem.* **204,** 1165–1168
26. Kabsch, W. (2010) XDS. *Acta Crystallogr. D Biol. Crystallogr.* **66,** 125–132
27. Vagin, A., and Teplyakov, A. (2010) Molecular replacement with MOLREP. *Acta Crystallogr. D Biol. Crystallogr.* **66,** 22–25
28. Winn, M. D., Ballard, C. C., Cowtan, K. D., Dodson, E. J., Emsley, P., Evans, P. R., Keegan, R. M., Krissinel, E. B., Leslie, A. G., McCoy, A., McNicholas, S. J., Murshudov, G. N., Pannu, N. S., Potterton, E. A., Powell, H. R., Read, R. J., Vagin, A., and Wilson, K. S. (2011) Overview of the CCP4 suite and current developments. *Acta Crystallogr. D Biol. Crystallogr.* **67,** 235–242
29. Murshudov, G. N., Vagin, A. A., and Dodson, E. J. (1997) Refinement of macromolecular structures by the maximum-likelihood method. *Acta Crystallogr. D Biol. Crystallogr.* **53,** 240–255
30. Emsley, P., and Cowtan, K. (2004) Coot: model-building tools for molecular graphics. *Acta Crystallogr. D Biol. Crystallogr.* **60,** 2126–2132
31. Chen, V. B., Arendall, W. B., 3rd, Headd, J. J., Keedy, D. A., Immormino, R. M., Kapral, G. J., Murray, L. W., Richardson, J. S., and Richardson, D. C. (2010) MolProbity. All-atom structure validation for macromolecular crystallography. *Acta Crystallogr. D Biol. Crystallogr.* **66,** 12–21
32. Hayward, S., and Lee, R. A. (2002) Improvements in the analysis of domain motions in proteins from conformational change: DynDom Version 1.50. *J. Mol. Graph. Model* **21,** 181–183
33. Krissinel, E., and Henrick, K. (2007) Inference of macromolecular assemblies from crystalline state. *J. Mol. Biol.* **372,** 774–797
34. Schiefner, A., Gerber, K., Seitz, S., Welte, W., Diederichs, K., and Boos, W. (2005) The crystal structure of Mlc, a global regulator of sugar metabolism in *Escherichia coli*. *J. Biol. Chem.* **280,** 29073–29079
35. Weihofen, W. A., Berger, M., Chen, H., Saenger, W., and Hinderlich, S. (2006) Structures of human *N*-acetylglucosamine kinase in two complexes with *N*-acetylglucosamine and with ADP/glucose. Insights into substrate specificity and regulation. *J. Mol. Biol.* **364,** 388–399
36. Nishimasu, H., Fushinobu, S., Shoun, H., and Wakagi, T. (2007) Crystal structures of an ATP-dependent hexokinase with broad substrate specificity from the hyperthermophilic archaeon *Sulfolobus tokodaii*. *J. Biol. Chem.* **282,** 9923–9931
37. Nocek, B., Stein, A. J., Jedrzejczak, R., Cuff, M. E., Li, H., Volkart, L., and Joachimiak, A. (2011) Structural studies of ROK fructokinase YdhR from *Bacillus subtilis*. Insights into substrate binding and fructose specificity. *J. Mol. Biol.* **406,** 325–342
38. Sinev, M. A., Sineva, E. V., Ittah, V., and Haas, E. (1996) Domain closure in adenylate kinase. *Biochemistry* **35,** 6425–6437
39. Titgemeyer, F., Reizer, J., Reizer, A., and Saier, M. H., Jr. (1994) Evolutionary relationships between sugar kinases and transcriptional repressors in bacteria. *Microbiology* **140**, 2349–2354
40. Hansen, T., Reichstein, B., Schmid, R., and Schönheit, P. (2002) The first archaeal ATP-dependent glucokinase, from the hyperthermophilic crenarchaeon *Aeropyrum pernix*, represents a monomeric, extremely thermophilic ROK glucokinase with broad hexose specificity. *J. Bacteriol.* **184,** 5955–5965
41. Mesak, L. R., Mesak, F. M., and Dahl, M. K. (2004) *Bacillus subtilis* GlcK activity requires cysteines within a motif that discriminates microbial glucokinases into two lineages. *BMC Microbiol.* **4,** 6
42. Ghaderi, D., Strauss, H. M., Reinke, S., Cirak, S., Reutter, W., Lucka, L., and Hinderlich, S. (2007) Evidence for dynamic interplay of different oligomeric states of UDP-*N*-acetylglucosamine 2-epimerase/*N*-acetylmannosamine kinase by biophysical methods. *J. Mol. Biol.* **369,** 746–758
43. Petit, P., Antoine, M., Ferry, G., Boutin, J. A., Lagarde, A., Gluais, L., Vincentelli, R., and Vuillard, L. (2011) The active conformation of human glucokinase is not altered by allosteric activators. *Acta Crystallogr. D Biol. Crystallogr.* **67,** 929–935
44. Lunin, V. V., Li, Y., Schrag, J. D., Iannuzzi, P., Cygler, M., and Matte, A. (2004) Crystal structures of *Escherichia coli* ATP-dependent glucokinase and its complex with glucose. *J. Bacteriol.* **186,** 6915–6927
45. Aleshin, A. E., Kirby, C., Liu, X., Bourenkov, G. P., Bartunik, H. D., Fromm, H. J., and Honzatko, R. B. (2000) Crystal structures of mutant monomeric hexokinase I reveal multiple ADP-binding sites and conformational changes relevant to allosteric regulation. *J. Mol. Biol.* **296,** 1001–1015
46. Cordeiro, A. T., Cáceres, A. J., Vertommen, D., Concepción, J. L., Michels, P. A., and Versées, W. (2007) The crystal structure of *Trypanosoma cruzi* glucokinase reveals features determining oligomerization and anomer specificity of hexose-phosphorylating enzymes. *J. Mol. Biol.* **372,** 1215–1226
47. Dennis, J. W., and Laferte, S. (1987) Tumor cell surface carbohydrate and

the metastatic phenotype. *Cancer Metastasis Rev.* **5,** 185–204
48. Stolz, F., Reiner, M., Blume, A., Reutter, W., and Schmidt, R. R. (2004) Novel UDP-glycal derivatives as transition state analogue inhibitors of UDP-GlcNAc 2-epimerase. *J. Org. Chem.* **69,** 665–679
49. Al-Rawi, S., Hinderlich, S., Reutter, W., and Giannis, A. (2004) Synthesis and biochemical properties of reversible inhibitors of UDP-*N*-acetylglucosamine 2-epimerase. *Angew. Chem. Int. Ed. Engl.* **43,** 4366–4370
50. Hinderlich, S., Berger, M., Schwarzkopf, M., Effertz, K., and Reutter, W. (2000) Molecular cloning and characterization of murine and human *N*-acetylglucosamine kinase. *Eur. J. Biochem.* **267,** 3301–3308
51. Roseman, S. (1970) The synthesis of complex carbohydrates by multiglycosyltransferase systems and their potential function in intercellular adhesion. *Chem. Phys. Lipids* **5,** 270–297
52. Lawrence, S. M., Huddleston, K. A., Pitts, L. R., Nguyen, N., Lee, Y. C., Vann, W. F., Coleman, T. A., and Betenbaugh, M. J. (2000) Cloning and expression of the human *N*-acetylneuraminic acid phosphate synthase gene with 2-keto-3-deoxy-D-glycero-D-galacto-nonionic acid biosynthetic ability. *J. Biol. Chem.* **275,** 17869–17877